Earth and Planetary Science Letters 567 (2021) 116984

Contents lists available at ScienceDirect

Earth and Planetary Science Letters

www.elsevier.com/locate/epsl

Atmospheric controls on precipitation isotopes and hydroclimate in high-elevation regions in Eastern Africa since the Last Glacial Maximum

Sloane Garelick [a,*], James M. Russell [a], Sylvia Dee [b], Dirk Verschuren [c], Daniel O. Olago [d,e]

[a] Department of Earth, Environmental and Planetary Sciences, Brown University, Providence, RI, United States of America
[b] Department of Earth, Environmental and Planetary Sciences, Rice University, Houston, TX, United States of America
[c] Department of Biology, Limnology Unit, Ghent University, Ghent, Belgium
[d] Department of Geology, University of Nairobi, Nairobi, Kenya
[e] Institute for Climate Change and Adaptation, University of Nairobi, Nairobi, Kenya

ARTICLE INFO

Article history:
Received 10 September 2020
Received in revised form 22 April 2021
Accepted 30 April 2021
Available online 25 May 2021
Editor: Y. Asmerom

Keywords:
East Africa
hydrogen isotopes
high-elevation climate
precipitation
lapse rate

ABSTRACT

Tropical Africa experienced large changes in hydroclimatic conditions since the Last Glacial Maximum (LGM), ~26.5 to 19 thousand years (ka or kyr) ago. The hydrogen isotopic composition of fossil leaf waxes (δD_{wax}), assumed to record past variations in the hydrogen isotopic composition of precipitation (δD_{precip}), is increasingly being used to study past hydroclimatic change in Africa, and are commonly interpreted to reflect variation in the amount of precipitation through time (i.e., the amount effect). Although there are now many such δD_{precip} records from tropical Africa, there are few robust δD_{precip} records from easternmost equatorial Africa of sufficient length and resolution to evaluate the mechanisms governing hydroclimate variation during and since the LGM. We produced a new δD_{precip} record based on analyses of δD_{wax} in sediment cores collected from Lake Rutundu, situated at an elevation of 3,078 meters above sea level (m asl) on Mt. Kenya. This record displays large variations in δD_{precip} corresponding with known climate events over the past 25 kyr, including D-enrichment during the Heinrich 1 stadial (H1) and the Younger Dryas (YD), and D-depletion during the Holocene portion of the African Humid Period (AHP). We also observe D-depletion during the LGM relative to the late Holocene, which, considering the amount effect, could be interpreted to imply that LGM climate conditions were wetter than today. However, because other hydroclimate proxies at this site indicate a drier LGM climate at Lake Rutundu, and since precipitation isotopes at this high-elevation site are likely influenced by different processes than at low elevations, we used a single-column Rayleigh distillation model to evaluate temperature and altitude-related effects on high-elevation δD_{precip}. This revealed that a change in the temperature lapse rate exerts strong control on δD_{precip} in this high-elevation setting, and that a steeper lapse rate could explain the observed D-depletion during the LGM at our site. Comparison of the Lake Rutundu δD_{precip} record with other leaf-wax based δD_{precip} records from East Africa indicates that changes in the meridional precipitation gradient associated with the mean annual position and intensity of the tropical rain belt, in turn driven by precessional insolation forcing, were likely a primary control on East African hydroclimate over the past 25 kyr, thereby contributing to overall regional drying during the LGM.

1. Introduction

Eastern equatorial Africa is predicted to experience significant changes in precipitation regimes as greenhouse-gas concentrations rise and the climate warms (Niang et al., 2014). Precipitation is critical to agriculture, food and water security, and power generation, yet many areas of East Africa are ill-equipped to adapt to the potential impacts of either increasing or decreasing average rainfall. The fact that climate models disagree on the sign of their projections for future rainfall in this region highlights the need for improved understanding of the controls on regional rainfall (Niang et al., 2014). To help improve climate-model performance, reconstructions of East African climate regimes under different boundary conditions in the past are important because they can provide constraints on regional climate dynamics and their governing mechanisms.

* Corresponding author.
E-mail address: sloane_garelick@brown.edu (S. Garelick).

https://doi.org/10.1016/j.epsl.2021.116984
0012-821X/

The Last Glacial Maximum (LGM; ~26.5-19 ka) and subsequent deglaciation is an important target for understanding future climate changes because it is the most recent time when global warming was accompanied by a large increase in atmospheric greenhouse-gas concentrations. Previous proxy reconstructions and modeling have provided abundant evidence that substantial variation in African hydroclimate has occurred since the LGM, but there is still disagreement surrounding past trends in hydroclimate and associated controlling mechanisms at the regional scale. Many reconstructions and regional syntheses indicate that most of northern and tropical Africa was drier during the LGM than during the late Holocene, including the present (e.g., Gasse, 2000; Otto-Bliesner et al., 2014; Tierney et al., 2008). Mechanisms proposed to explain this drying include lower sea surface temperatures (SST) in the adjacent tropical oceans, which decreased evaporation and lowered atmospheric water-vapor content (Gasse, 2000; Otto-Bliesner et al., 2014); southward migration of the Intertropical Convergence Zone (ITCZ) in response to decreased northern hemisphere (NH) temperature and expanded NH ice sheets (Otto-Bliesner et al., 2014); and weakened atmospheric convection in response to continental cooling (e.g., Tierney et al., 2008). However, several studies suggest that at least part of easternmost tropical Africa was wetter during the LGM than during the late Holocene (e.g., DiNezio et al., 2018; Garcin et al., 2006; Verschuren et al., 2009), potentially due to a response of the Indian Ocean Walker Circulation to exposure of continental shelves in the Indo-Pacific Warm Pool (IPWP) region during the LGM (DiNezio et al., 2018). Understanding to what extent East African hydrology during and after the LGM was affected by meridional versus zonal changes in atmospheric circulation is crucial for resolving this apparent regional contrast in the reconstructions.

It has been challenging to diagnose the controls on tropical African rainfall from the existing East African hydroclimate records. There is disagreement between records from the same region, and sometimes between different proxy records from the same site. For example, the diatom-based salinity record from Lake Masoko (Tanzania) indicates saline conditions during the LGM, consistent with a drier climate (Barker and Gasse, 2003), whereas magnetic susceptibility and palynological data from the same lake suggest a wetter and/or more seasonal climate (Garcin et al., 2006). Chronological uncertainties also influence many existing records. For example, the water-level reconstruction from Lake Abhé (Ethiopia), based on radiocarbon dating of exposed shorelines, originally suggested wet LGM conditions, until additional dating constraints from lake low-stand deposits indicated drying (Barker and Gasse, 2003).

Regional comparison of paleorecords across East Africa is often complicated by the use of different proxies to infer the same climate variable (e.g., precipitation) at different sites. An alternative approach is to measure a single proxy in the largest-possible number of well-dated sediment archives across Africa. One promising proxy for this purpose is the compound-specific hydrogen isotopic composition of leaf waxes (δD_{wax}) from terrestrial vascular plants, which are transported to lakes via wind or water and preserved in bottom sediments (Sachse et al., 2012). δD_{wax} reflects the hydrogen isotopic composition of precipitation, $\delta D_{precip,}$ (Sachse et al., 2012), making it a valuable proxy for reconstructing past variation in hydroclimate and its governing atmospheric processes across Africa (e.g., Costa et al., 2014; Shanahan et al., 2015).

δD_{precip} records from tropical regions are traditionally interpreted to reflect the amount of precipitation, with more depleted δD_{precip} values indicating increased precipitation (i.e., the amount effect; Dansgaard, 1964; Sachse et al., 2012). However, multiple processes such as moisture source, convective intensity, and other phenomena associated with water-vapor transport, condensation and precipitation, have been proposed to also influence δD_{precip} (e.g., Costa et al., 2014; Konecky et al., 2011). Therefore, a large number of such δD_{precip} records is needed to distinguish between primary and secondary controls at different scales of time and space. Although the geographic coverage of leaf-wax based δD_{precip} records across Africa is steadily increasing (Fig. 1A), there are comparatively few robust records from easternmost equatorial Africa (Fig. 1B), a region in which some models predict strong impacts of shelf exposure-driven changes in the Walker Circulation and wetter conditions during the LGM (DiNezio et al., 2018). The δD record from Lake Chala (Tierney et al., 2011), located in this region, was originally interpreted to reflect δD_{precip} but recent work indicates that this record may be compromised because the measured C_{28} *n*-acid compound is likely derived from aquatic plants (e.g., phytoplankton) within Lake Chala rather than terrestrial plants (Van Bree et al., 2018). δD values measured from aquatically sourced *n*-acid compounds likely don't reflect δD_{precip} due to differences in biosynthetic fractionation and source-water δD relative to terrestrially compounds. Thus, additional δD_{precip} records from easternmost equatorial Africa are required to assess hydroclimate conditions in this easternmost portion of the continent relative to other regions during the LGM.

We here present a 25 thousand-year (kyr) record of δD_{precip} from Lake Rutundu, a relatively high-elevation lake on Mt. Kenya in easternmost equatorial Africa. We compare this record with data from other precipitation-sensitive proxies from Mt. Kenya (Ficken et al., 2002; Wooller et al., 2003) as well as with δD_{precip} records from throughout East Africa. We evaluate the controls on δD_{precip} in this high-elevation, tropical setting using a single-column Rayleigh distillation model. Finally, we summarize new insights gained from this record to explore the atmospheric processes that have controlled East African precipitation since the LGM.

2. Study site

Lake Rutundu is a small maar crater lake situated at 3,078 meters above sea level (m asl) on the eastern slope of Mt. Kenya, almost exactly on the equator (0.0412° S, 37.4635° E). The lake is a fresh, oligotrophic lake with a surface area of 0.4 km^2 and maximum depth of 11 m (Ficken et al., 2002). Modern-day vegetation on Mt. Kenya is characterized by three major vegetation zones along an altitudinal gradient: montane forest, ericaceous forest and afroalpine grassland (Konecky et al., 2014a). Lake Rutundu is located in the ericaceous belt, which primarily consists of C_3 subalpine shrubs and grasses (Ficken et al., 2002). Today, the mean annual air temperature at this elevation is 12 °C (Loomis et al., 2017), and given the site's equatorial location, the seasonal variation in temperature is minimal. The northeastern flank of Mt. Kenya where Lake Rutundu is located receives ~1500 mm of precipitation per year (Ficken et al., 2002), mostly during the rainy seasons from March to June (long rains) and October to November (short rains). This bimodal rainfall seasonality reflects the twice-yearly passage of the tropical rain belt associated with the ITCZ across the equator (Konecky et al., 2014a). The primary moisture source for both rainy seasons is the Indian Ocean (Konecky et al., 2014a).

Seasonal to interannual variation in precipitation in this part of East Africa is not only controlled by the relationship between Indian Ocean monsoon dynamics and latitudinal migration of the ITCZ, but also by variations in zonal Walker Circulation and the phase of the Indian Ocean Dipole (IOD), all of which vary with changes in equatorial Indian Ocean SST (Konecky et al., 2014a,b). Therefore, precipitation over the Lake Rutundu catchment is particularly sensitive to changes in water cycling over the Indian Ocean and related hydroclimate processes (Konecky et al., 2014a). Previous work has shown that there is a strong positive correla-

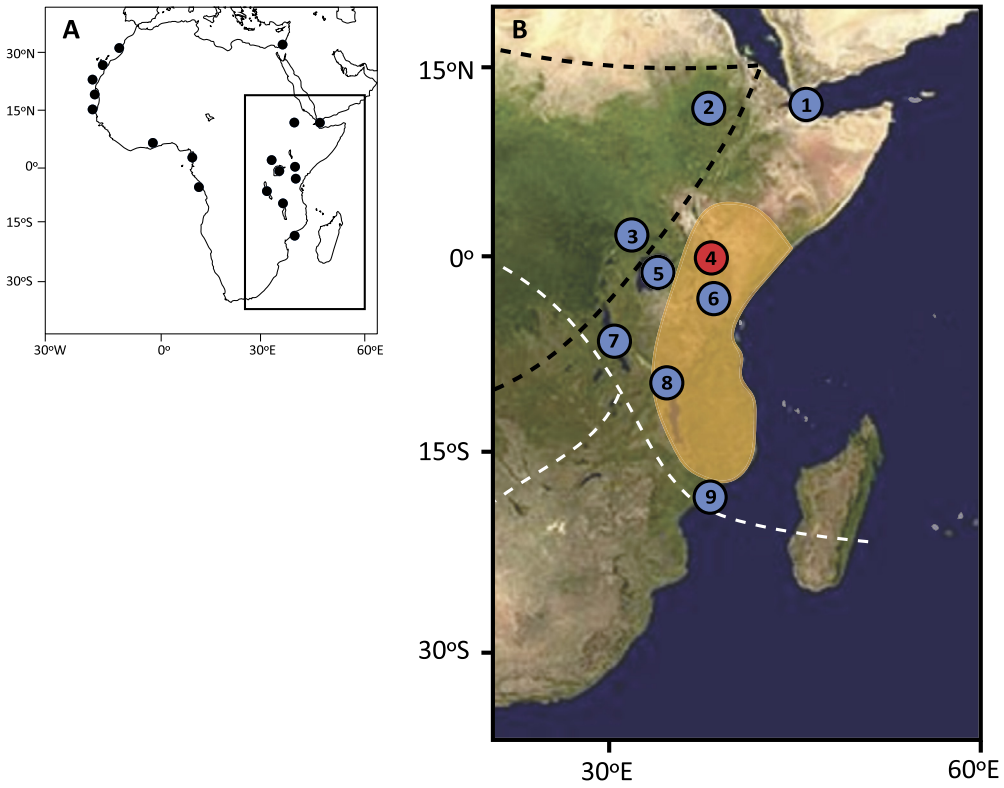

Fig. 1. A) Locations of existing δD_{precip} records from Africa. B) Detailed map of existing δD_{precip} records in East Africa, from the Gulf of Aden (1; Tierney and deMenocal, 2013), Lake Tana (2; Costa et al., 2014), Lake Albert (3; Berke et al., 2014), Lake Victoria (5; Berke et al., 2012), Lake Chala (6; Tierney et al., 2011), Lake Tanganyika (7; Tierney et al., 2008), Lake Malawi (8; Konecky et al., 2011) and the Zambezi River Delta (9; Schefuß et al., 2011). Lake Rutundu on Mt. Kenya (4; this study) is plotted in red. The approximate location of the Intertropical Convergence Zone (ITCZ) and Congo Air Boundary (CAB) during Northern Hemisphere Summer (JJA; black dashed line) and Southern Hemisphere Summer (DJF; white dashed line) are also shown. The yellow-shaded area represents the region we define as easternmost equatorial Africa, where some models predict a wetter LGM (DiNezio et al., 2018). (For interpretation of the colors in the figure(s), the reader is referred to the web version of this article.)

tion between East African precipitation isotopes and zonal wind anomalies (Vuille et al., 2005), including at sites on Mt. Kenya near Lake Rutundu (Konecky et al., 2014b). Because zonal wind anomalies are tied to the IOD, changes in δD_{precip} in this region should record changes in precipitation amounts and the strength of the Walker Circulation over the Indian Ocean (Vuille et al., 2005), at least on relatively short time scales.

Lake Rutundu is the highest-elevation site among existing African δD_{precip} records. It is located above the modern lifting condensation level (LCL), the elevation at which an air parcel becomes saturated and precipitation forms, which today in tropical regions is at approximately 1,000 m above the land surface, or approximately 2,000 m asl throughout most of East Africa (Chen et al., 2020). As a result, Rayleigh distillation during upslope vapor transport and condensation will result in D-depletion of precipitation (i.e., the elevation effect) at Lake Rutundu compared to lower elevations (Rowley and Garzione, 2007). In addition, this D-depletion is likely compounded by elevation-dependent temperature influences on isotopic fractionation (Rowley and Garzione, 2007). These factors must be evaluated to clarify the controls on the leaf-wax based δD_{precip} record from Lake Rutundu.

3. Methods

3.1. Sample preparation and analysis

We measured the hydrogen isotopic composition of long-chain *n*-alkanes, derived from the leaf waxes of terrestrial plants (Sachse et al., 2012) that grew around Lake Rutundu. These *n*-alkanes were extracted from discrete samples of two lake-sediment cores collected from the deepest part of Lake Rutundu: Rut09, a 3.2-meter-long composite core collected in 2009 (Loomis et al., 2017) and Rut96, a 7.55-meter-long core collected in 1996 (Ficken et al., 2002). The age model of Rut09 is based on 19 radiocarbon ages and a ^{210}Pb-profile with 10 dated intervals, and accounts for one tephra layer and two turbidites (Loomis et al., 2017). The age model of Rut96 is based on 16 radiocarbon ages (Ficken et al., 2002). Loomis et al. (2017) stratigraphically aligned these two cores based upon their radiocarbon ages as well as profiles of total organic carbon concentration, the carbon isotopic composition of organic matter, and magnetic susceptibility. This resulted in a continuous sediment sequence spanning the past 25 kyr.

Our δD_{precip} reconstruction is based on the hydrogen isotopic composition of long-chain *n*-alkanes extracted from Lake Rutundu sediments. Procedures used for lipid extraction and purification are similar to those presented in Schefuß et al. (2011). Sediment samples (56 total) were freeze-dried and lipids were extracted using a DIONEX Accelerated Solvent Extractor with dichloromethane:methanol (DCM:MeOH, 9:1). The lipids were separated into neutral and acid fractions using aminopropylsilyl gel columns with DCM:isopropoanol (2:1) and ether:acetic acid (24:1). The neutral fractions, containing the *n*-alkanes, were further separated into polar and non-polar compounds using silica gel columns with hexane, DCM and MeOH. For select samples, the hexane fraction containing the *n*-alkanes was further purified on a silver thiolate column with hexane and acetone to separate the saturated and unsaturated hydrocarbons. Relative abundances of *n*-alkanes in all hexane fractions were quantified using an Agilent 6890 gas chromatograph (GC) with an HP1-MS column (30 m $\times$ 0.25 mm $\times$ 0.25 µm) and flame ionization detector (FID). Based on these abundances, we calculated the average chain length (ACL), which can indicate changes in the type of vegetation producing the leaf-

wax *n*-alkanes (Cranwell, 1973), and the carbon preference index (CPI), which can indicate plant source and degradation (Bray and Evans, 1961).

δD_{wax} was measured in triplicate on an Agilent 6890 GC with an HP1-MS column (30 m × 0.25 mm × 0.25 µm), coupled to a Thermo Delta Plus XL isotope-ratio mass spectrometer (IRMS) with a reactor temperature of 1445 °C. Samples were calibrated to a reference hydrogen gas of known isotopic composition and are reported relative to Vienna Standard Mean Ocean Water (VSMOW). An internal standard consisting of a set of fatty acid methyl esters (FAMEs) was measured after every nine sample injections to monitor instrument drift. The H3 factor was 1.778 during the analyses, suggesting no or minimal fluctuation in IRMS performance. Measured isotopic values were accepted if the voltage was between 2.5 and 8 V. We focus our discussion on δD_{wax} values of the C_{29} *n*-alkane, yet the C_{27} and C_{31} homologues were also measured on 46 of the 56 samples (Supplementary Figure 1). Triplicate C_{29} δD_{wax} values for each sample had an average 1σ error of 1.04‰ with a maximum 1σ error of 3.33‰. The other two homologues showed similar down-core trends as those of C_{29}, with C_{27} showing the greatest correlation ($r^2 = 0.532$) and C_{31} showing slightly weaker correlation ($r^2 = 0.402$) (Supplementary Figure 1).

Different plant types fractionate hydrogen isotopes differently, resulting in different apparent fractionations ($\varepsilon_{wax\text{-}P}$) between δD_{precip} and δD_{wax} (Sachse et al., 2012). At our site, we specifically needed to account for the effect of changes in the proportion of montane C_3 plants versus C_4 grasses in local vegetation. As in previous work (Konecky et al., 2016), we apply a vegetation correction that uses the carbon isotopic composition of the leaf waxes ($\delta^{13}C_{wax}$) to define the abundance ratio between C_3 and C_4 plants that contributed waxes to Lake Rutundu, and correct the δD_{wax} using Equation (1) (Konecky et al., 2016).

$$\varepsilon_{wax-P} = \left(fC_3 \times \varepsilon_{C27.alk-P_{C3}}\right) + \left(fC_4 \times \varepsilon_{C27.alk-P_{C4}}\right) \quad (1)$$

The values for $\varepsilon_{C27.alk-P_{C3}}$ and $\varepsilon_{C27.alk-P_{C4}}$ used in Equation (1) are the average apparent fractionation of C_{27} *n*-alkanes for C_3 and C_4 plants, −128.9‰ and −125.4‰, respectively, identified by Konecky et al. (2016) as the average end members for tropical vegetation (i.e., between 30° N and 30° S). fC_3 and fC_4 are the fraction of C_3 and C_4 plants contributing leaf waxes to each sample, calculated using the linear mixing model described by Equations (2) and (3) (Uno et al., 2016).

$$fC_3 = \frac{(\delta^{13}C_{sample} - \delta^{13}C_{C4})}{(\delta^{13}C_{C3} - \delta^{13}C_{C4})} \quad (2)$$

$$fC_4 = 1 - fC_3 \quad (3)$$

In Equation (2), $\delta^{13}C_{C3}$ and $\delta^{13}C_{C4}$ are $\delta^{13}C_{wax}$ end-member values for C_3 and C_4 plants. We used the *n*-alkane end-member values specific for East Africa proposed by Uno et al. (2016), which are −31.1‰ for C_3 and −19‰ for C_4. For $\delta^{13}C_{sample}$ values, we used $\delta^{13}C_{wax}$ values from the Rut96 core measured by Wooller et al. (2003), which we interpolated to our time series of δD_{wax} (Fig. 2A). $\delta^{13}C_{wax}$ is relatively constant over the past 25 kyr, with an average value of −28.68‰ and average 1σ error of 1.84‰, suggesting minimal vegetation change. To evaluate the influence of this method of δD_{wax} correction, we calculated δD_{precip} by estimating time-varying $\varepsilon_{wax\text{-}P}$ values in which vegetation change was inferred from fossil pollen data (Ficken et al., 2002), and also calculated δD_{precip} using a time-invariant $\delta^{13}C_{wax}$ value from recent sediments.

The vegetation-corrected δD_{wax} values were then corrected for the effect of long-term changes in global land-ice volume on the average δD of seawater. This was done by scaling the ice-volume changes reflected by the LR04 benthic oxygen-isotope stack

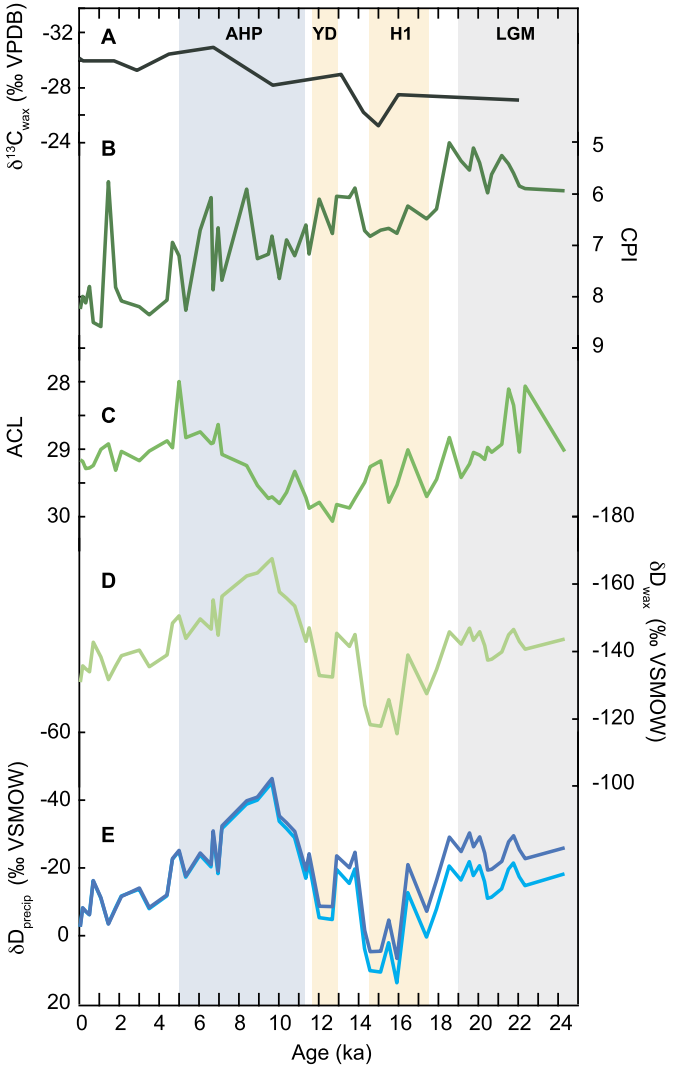

Fig. 2. Leaf-wax based proxy records from Lake Rutundu over the past 25 kyr. The timing of the Holocene portion of the AHP (11-5 ka), YD (12.9-11.6 ka) and H1 stadial (17.5-14.5 ka) are noted with shading indicating a traditionally wetter climate (blue) or drier climate (yellow). The timing of the LGM is shaded in gray. A) Record of $\delta^{13}C_{wax}$ from the Rut96 core (Wooller et al., 2003) used to correct the δD_{wax} data for changes in vegetation composition. B) Carbon preference index (CPI). C) Average chain length (ACL). D) Raw δD_{wax} time series. E) Time series of δD_{precip} from Lake Rutundu as derived from the δD_{wax} data after correction for vegetation changes (light blue line) and correction for changes in both vegetation and global ice volume (dark blue line).

(Lisiecki and Raymo, 2005) to pore-water analyses indicating that the LGM ocean $\delta^{18}O$ was 1‰ more enriched than today (Schrag et al., 2002), and relating this to our δD record through the global meteoric water line (Dansgaard, 1964). Following these two corrections, our δD_{wax} values are interpreted to represent δD_{precip} over the Lake Rutundu catchment at the time of leaf-wax formation and their incorporation in the sediment record. We applied the same vegetation and ice-volume corrections to the published East African δD_{wax} records, allowing for their direct comparison with our Lake Rutundu δD_{precip} record (Supplementary Figure 2 and Supplementary Table 2).

3.2. Single-column Rayleigh distillation model

We used a single-column Rayleigh distillation model (Dee et al., 2018) to assess how changes in temperature with elevation may impact δD_{precip} at high-elevation Lake Rutundu. This model was initialized with observed values for surface temperature at

Table 1
Summary of variables describing the initial conditions of the single-column Rayleigh distillation model and the variables produced by model output.

Model initial conditions	
Variable	Term
T	Surface temperature
Γ	Temperature lapse rate
δD_v	Hydrogen-isotopic composition of water vapor*
Model outputs	
Variable	Term
q	Specific humidity
$\alpha(T)$	Temperature-dependent equilibrium fractionation factor
δD_v	Hydrogen-isotopic composition of water vapor
$\delta D_{produced}$	Hydrogen-isotopic composition of precipitation *produced at* each elevation
δD_{precip}	Hydrogen-isotopic composition of precipitation *falling at* each elevation

*Only the surface δD_v is an initial condition; δD_v elevation profiles are calculated by the model.

Table 2
Initial conditions for the three climate scenarios run in the single-column Rayleigh distillation model. Surface temperature values (T) are based on modern observational surface temperatures in eastern equatorial Africa (Loomis et al., 2017) and an estimated cooling of ~3 °C at low-elevation sites in this region during the LGM. Modern and LGM temperature lapse rates (Γ) are based on results presented in Loomis et al. (2017). The surface δD_v value is a regional average of SCIAMACHY data (Frankenberg et al., 2009).

Climate scenario	T (°C)	Γ (°C/km)	Surface δD_v (‰)
Modern surface T, modern Γ	25	−5.8	−85
LGM surface T, modern Γ	22	−5.8	−85
LGM surface T, LGM Γ	22	−6.7	−85

sea level (hereafter, surface temperature; T), temperature lapse rate (i.e., the decrease in temperature with increasing elevation; Γ) and the surface hydrogen isotopic composition of water vapor (δD_v; Table 1) to calculate profiles of δD_{precip} versus elevation above the surface for three different climate scenarios: 'modern surface T, modern Γ', 'LGM surface T, modern Γ' and 'LGM surface T, LGM Γ' (Table 2). These three climate scenarios are intended to assess differences in elevation-dependent isotopic fractionation under different climate states by determining the influence of changes in surface temperature and/or temperature lapse rate on the isotopic composition of precipitation at different elevations. Surface δD_v values were set to −85‰ for all three climate scenarios, based on the average value of Scanning Imaging Absorption Spectrometer for Atmospheric Chartography (SCIAMACHY) data over East Africa (Frankenberg et al., 2009; Table 2). We recognize that δD_v was likely different during the LGM, but our goal is to examine the effects of changes in atmospheric temperature. Modern-day mean-annual surface temperature in eastern equatorial Africa is ~25 °C, and cooling during the LGM relative to today is estimated to have been ~3 °C at the surface (Loomis et al., 2017). Based on these results, we used a surface temperature of 25 °C for our 'modern surface T, modern Γ' simulation, and a surface temperature of 22 °C for our 'LGM surface T, modern Γ' and 'LGM surface T, LGM Γ' scenarios (Table 2).

We note that the temperature lapse rate in tropical regions during the LGM is uncertain. While climate-model simulations indicate it was similar to the modern-day value of −5.8 °C/km, temperature proxy records based on branched glycerol dialkyl glycerol tetraethers (brGDGTs) along an elevational gradient in East Africa indicate a temperature lapse rate of −6.7 °C/km during the LGM (Loomis et al., 2017). These authors suggested that the colder LGM atmosphere likely had less moisture, which created a steeper temperature lapse rate. Based on these results, we consider two possible LGM temperature lapse rates: in our 'modern surface T, modern Γ' and 'LGM surface T, modern Γ' scenarios we use a modern lapse rate value of −5.8 °C/km, and in our 'LGM surface T, LGM Γ' scenario we us an LGM lapse rate value of −6.7 °C/km (Table 2).

Using these input values (Table 2), the Rayleigh-distillation model generated profiles of specific humidity (q), the temperature-dependent equilibrium fractionation factor ($\alpha(T)$), and δD_v at different elevations in the atmosphere (Table 1). From these model outputs, we calculated the respective hydrogen isotopic composition of precipitation produced at each elevation ($\delta D_{produced}$; Table 1) using Equation (4), similar to one presented by Rowley and Garzione (2007).

$$\delta D_{produced} = \alpha(T) \times (\delta D_v + 1000) - 1000 \quad (4)$$

However, the calculated isotopic composition of precipitation produced at a given elevation does not accurately reflect the total precipitation falling at that elevation due to contributions from higher atmospheric levels. For example, the precipitation falling at 3,000 m asl includes D-depleted precipitation from 4,000 m asl and higher. To account for this, we calculated the hydrogen isotopic composition of precipitation falling at a given elevation (δD_{precip}; Table 1) by weighting the difference between $\delta D_{produced}$ at that elevation and one elevation higher by the difference in q, to represent the amount of precipitation forming between those two elevations and then summing these values over all elevations higher than the given elevation. Fractionation does not occur in the model until precipitation forms, above the LCL elevation of 2,000 m asl.

4. Results and discussion

4.1. Lake Rutundu δD_{precip} values

The CPI of our samples ranges from 5.00 to 8.58, with an average value of 6.72 (Fig. 2B). These CPI values are similar to those of modern African plants and well above 1, indicating good preservation of plant waxes in Lake Rutundu sediments (Bray and Evans, 1961). Although the CPI values display a sustained increasing trend from 18 ka towards the present, its magnitude is negligible with regard to the relative quality of preservation. Moreover, CPI is not correlated with δD_{wax} ($r^2 = 0.0731$), further suggesting a very weak influence of lipid degradation on isotopic composition. The ACL of the long-chain n-alkanes (C_{25} to C_{35}) ranges from 27.99 to 30.06 (on average 29.19; Fig. 2C), which reflects a predominantly terrestrial source of waxes to Lake Rutundu sediment (Cranwell, 1973). Additionally, a lack of correlation between ACL and δD_{wax} ($r^2 = 0.0037$) further indicates that the δD_{wax} signal at Lake Rutundu is not significantly influenced by changes in wax source.

Applying the vegetation correction based upon the full Lake Rutundu $\delta^{13}C_{wax}$ record to our δD_{wax} record resulted in an average apparent fractionation of −126.12‰ ($1\sigma = 1.54$‰) between δD_{wax} and δD_{precip} (Figs. 2D and 2E). Alternative methods of calculating the effect of vegetation change on δD_{precip} result in differences of less than 1‰ in $\varepsilon_{wax\text{-}P}$ (Supplementary Figure 3): vegetation correction based on the full $\delta^{13}C_{wax}$ record results in a −8.19‰ shift in δD_{precip} from the LGM to late Holocene (4-0 ka), whereas the vegetation correction based on fossil pollen data yields a shift of −8.27‰, and applying a constant modern $\delta^{13}C_{wax}$ value produces a −7.29‰ shift. The differences between these corrections are small and are within the analytical uncertainty of δD measurements, suggesting that our $\delta^{13}C_{wax}$-based correction accurately records vegetation change and can be used to convert from δD_{wax} to δD_{precip}.

The ice-volume correction of our δD_{precip} record had a limited effect throughout most of the Rutundu record, with a maximum

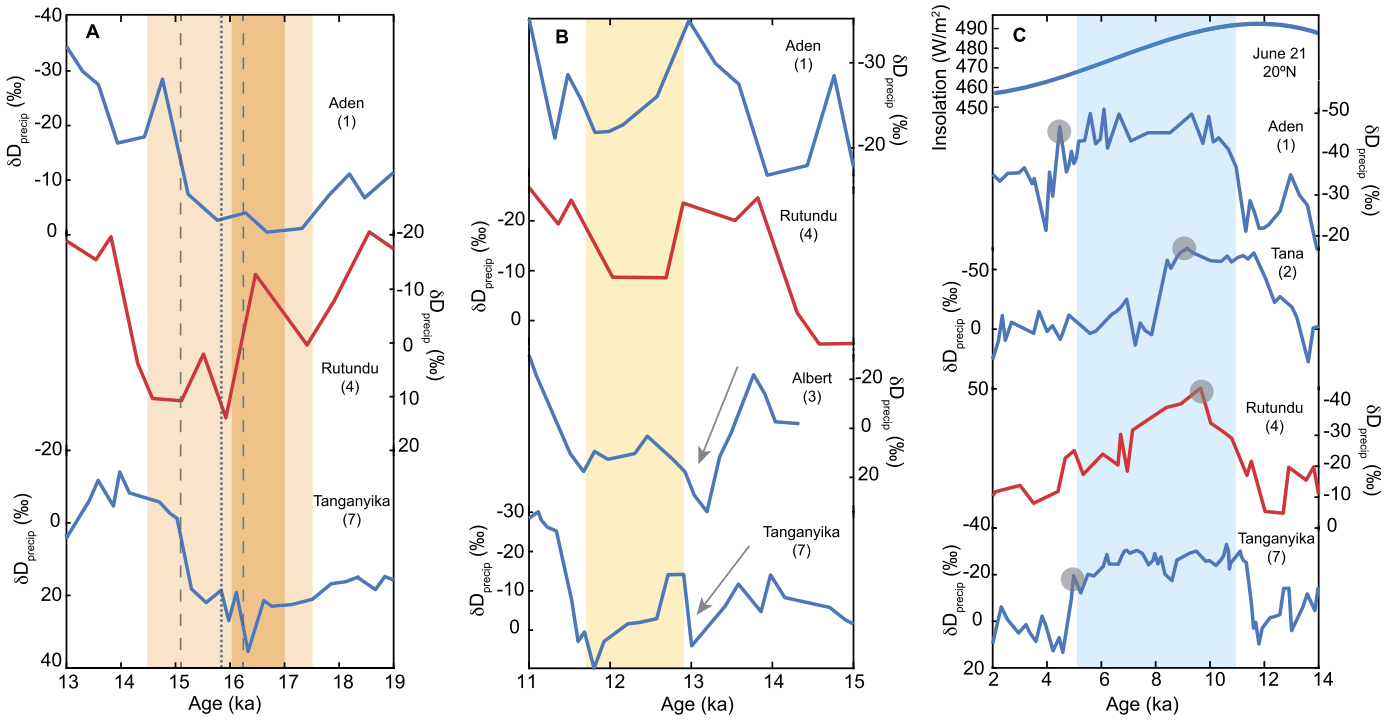

Fig. 3. Leaf-wax based δD_{precip} records, reported relative to VSMOW, from selected sites in East Africa highlighting the variations associated with millennial-scale climate events (A and B) and the Holocene trend (C). In each panel, records are numbered and plotted from north (top) to south (bottom), with reference to their site location in Fig. 1B, and our Lake Rutundu record plotted in red. A) The period 19-13 ka, highlighting variations associated with H1 stadial (17.5-14.5 ka; light orange shading); dark orange shading indicates the period of peak regional aridity, 17-16 ka (Stager et al., 2011). The dashed gray lines at ~15.1 ka and ~16.2 ka indicate the timing of H1 ice-rafting maxima in the North Atlantic Ocean (Hodell et al., 2017). The dotted gray line at ~15.8 ka indicates the timing of peak $\delta^{18}O$ depletion in the Hulu Cave speleothem record (Wang et al., 2001). B) The period 15-11 ka, highlighting variations associated with the YD (12.9-11. 6 ka; yellow shading). The gray arrows point to the D-enrichment from ~14 ka onwards observed in more western sites. C) The period 14-2 ka, highlighting the main Holocene trend in δD_{precip} in relation to NH Summer solstice insolation (June 21 at 20° N). The blue shading indicates the timing of the Holocene portion of the AHP (11-5 ka); gray circles indicate the approximate onset of AHP termination at each site.

depletion of ~8‰ occurring during the LGM (Fig. 2E). After applying both the vegetation and ice-volume corrections, the average modern (0.7-0 ka) δD_{precip} value is −8.12‰, which is similar to the average modern δD value for Kenyan surface waters in the 2,500-3,000 m asl elevation range (−10.9‰, calculated from the Water-isotopesDatabase, 2017). This similarity suggests that our δD_{precip} measurements are quantitatively reliable.

4.2. Late-Glacial millennial-scale hydroclimate events at Lake Rutundu

The 25-kyr δD_{precip} record from Lake Rutundu displays high-amplitude millennial-scale variability (Fig. 2E). There are notable intervals of D-enrichment corresponding with the timing of the Heinrich 1 stadial (H1) which occurred from ~17.5-14.5 ka (Hodell et al., 2017). For example, there is a period of D-enrichment at Lake Rutundu around 17.4 ka (Fig. 3A). Although temporary D-depletion at 16.5 ka follows this initial increase in δD_{precip}, given the sampling resolution, we cannot be sure that this temporary D-depletion represents a real episode of wetter climate. Following this, there is an interval of D-enrichment from ~16.4 to ~14.2 ka that includes two distinct peaks at about 15.9 and 15.1 ka (Fig. 3A). Assuming the amount effect was the primary control on δD_{precip} during this time, the timing of this event suggests an interval of drier conditions that may be attributable to the H1. Relatively dry conditions on Mt. Kenya during H1 are consistent with other climate proxy records from this time period in tropical Africa, indicating continental drying attributed to a weakening of the Indian Ocean monsoon system in response to cooler sea surface temperatures (Stager et al., 2011). However, not all existing leaf-wax based δD_{precip} records from East Africa record regional drying with a similar timing and structure to that recorded at Lake Rutundu. For example, δD_{precip} records from the Gulf of Aden region (Tierney and deMenocal, 2013) and Lake Tanganyika (Tierney et al., 2008) only record a modest D-enrichment at the onset of H1 compared to Lake Rutundu (Fig. 3A). Additionally, whereas Lake Rutundu exhibits two distinct peaks in D-enrichment, Lake Tanganyika D-enrichment is represented by a single value centered on ~16.3 ka (Fig. 3A). Although variations in sampling resolution and age model accuracy between the three records may partly explain these differences in δD_{precip} trends, the overall structure of the H1 anomaly in the Rutundu record clearly differs from that observed in Lake Tanganyika and the Gulf of Aden.

High-resolution analyses of North Atlantic deep-sea sediments suggest that H1 may have comprised two distinct ice-rafting events occurring at ~16.2 ka and ~15.1 ka (Hodell et al., 2017), with the earlier event being the larger of the two. An earlier synthesis of East African proxy records suggested that peak H1 aridity occurred between 16 ka and 17 ka (Stager et al., 2011), potentially predating the North Atlantic events. In the Hulu Cave $\delta^{18}O$ record (Wang et al., 2001), isotopic enrichment starts at 17.5 ka, and the interval of weakest South Asian monsoon strength is dated to 15.8 ka. Within the uncertainty of our age model (~214 years during H1) this is coeval with the strongest D-enrichment peak in our δD_{precip} record (at ~15.9 ka; Fig. 3A), suggesting considerable weakening of both the African and Asian monsoons at that time. Although the low sampling resolution of our δD_{precip} record during this interval makes it difficult to determine the exact timing of maximum drying, values remain enriched for ~1.5 kyr following this event, suggesting that dry conditions persisted after 15.9 ka. Moreover, the second-strongest D-enrichment peak in our record (~15.1-14.5 ka; Fig. 3A) is roughly coeval with the second pulse of North Atlantic ice-rafted debris centered at ~15.1 ka (Fig. 3A; Hodell et

al., 2017). We thus propose that the similarity in timing of these century-scale events indicates a strong atmospheric link between hydrological change in eastern equatorial Africa and North Atlantic climate dynamics.

Following H1, the Rutundu δD_{precip} record displays another short period of D-enrichment from 12.9 to 12 ka (Fig. 3B), suggesting drier conditions during the Younger Dryas (YD; 12.9-11.6 ka), another millennial-scale, NH high-latitude cooling event. Many climate-proxy records indicate relatively dry conditions in most of tropical East Africa during the YD (Gasse, 2000), possibly because the Indian Ocean monsoon was weakened by lower Indian Ocean SSTs associated with a slow-down in Atlantic Meridional Overturning Circulation (AMOC; Berke et al., 2014). However, δD_{precip} records from East Africa suggest that the timing and severity of drought during the YD varied regionally. Our Lake Rutundu δD_{precip} record exhibits an abrupt transition to more D-enriched values at 12.9 ka, similar to the timing of the onset of D-enrichment observed in the Gulf of Aden (Tierney and deMenocal, 2013; Fig. 3B) and to the onset of the YD itself as recorded in the oxygen-isotope record from Greenland ice cores (Svensson et al., 2008). In other East African δD_{precip} records, such as those from Lake Tanganyika (Tierney et al., 2008) and Lake Albert (Berke et al., 2014), D-enrichment began between 14 and 13.6 ka (Fig. 3B). Given the more western location of Lake Tanganyika and Lake Albert relative to Lake Rutundu and the Gulf of Aden, the former two sites are more directly affected by Atlantic moisture sources and the zonal migration of the Congo Air Boundary (CAB). Therefore, the difference in timing of D-enrichment between more eastern sites (i.e., Lake Rutundu and the Gulf of Aden), and more central sites (i.e., Lake Tanganyika and Lake Albert), may reflect short-lived drying over the western branch of the East African Rift Valley, possibly reflecting a weakening of the tropical Atlantic monsoon circulation that affected western and central Africa but not easternmost equatorial Africa. However, these differences in the timing of D-enrichment may in part be due to variations in the sampling resolution and age uncertainties between the records. The return to D-depleted values at the YD termination in Lake Rutundu occurs between 12.0 and 11.5 ka, which is similar to the timing of YD termination in the Gulf of Aden area within sample resolution or age-model uncertainty (~130 years during the YD), but slightly earlier than the YD termination at East African sites further west (Fig. 3B). This may indicate that the abrupt intensification of the Indian Ocean monsoon system at the YD termination (Talbot et al., 2007) resulted in rapid onset of moist conditions at Lake Rutundu and other East African sites.

4.3. Holocene hydroclimatic variation at Lake Rutundu

The substantial D-depletion marking the end of the YD at Lake Rutundu continued well into the early and mid-Holocene, with maximum depletion recorded at ~9.7 ka. This interval is consistent with wetter conditions corresponding to the timing of the Holocene portion of the African Humid Period (AHP, 11-5 ka; Fig. 3C). The AHP is recognized as a period of wet, humid conditions in northern and equatorial Africa, driven by intensification of the African monsoon due to orbitally-induced changes in seasonal insolation (Kutzbach and Otto-Bliesner, 1982). A regional synthesis of hydroclimate proxy records in northern and western equatorial Africa (Shanahan et al., 2015) found that the termination of the AHP in the early to mid-Holocene was regionally gradual but, in some cases, locally abrupt, as the tropical rain belt gradually migrated southwards. δD_{precip} records from several East African sites, such as the Gulf of Aden (Tierney and deMenocal, 2013), Lake Tana (Costa et al., 2014) and Lake Tanganyika (Tierney et al., 2008) suggest an abrupt termination of enhanced precipitation associated with the AHP (Fig. 3C). However, the δD_{precip} record from Lake Rutundu displays a more gradual decline in rainfall between 9.7 ka and the present (Fig. 3C). Nonlinear precipitation feedbacks in response to changes in insolation varied spatially across Africa and are thought to have been particularly pronounced in North Africa (Shanahan et al., 2015), so this gradual termination at Lake Rutundu may reflect its consistently vegetated, equatorial setting. However, equatorial sites further west, such as Lake Tanganyika, record an abrupt termination of the AHP (Fig. 3C), similar to east-west gradients observed elsewhere throughout Africa (Shanahan et al., 2015). This regional difference may suggest that rapid mid-Holocene change in the intensity of the Atlantic monsoon, which likely impacted central Africa (e.g., Lake Tanganyika), occurred alongside more gradual changes in Indian Ocean monsoon intensity, which dominated at equatorial sites in East Africa (e.g., Lake Rutundu). The gradual AHP termination observed at Lake Rutundu may also reflect a smaller magnitude of long-term vegetation changes relative to the more centrally located equatorial sites. Since moisture recycling over tropical forests varies with forest extent and can in turn affect the isotopic composition of precipitation (Ampuero et al., 2020), forest expansion in the Congo Basin during the AHP may have altered precipitation over more centrally-located sites (e.g., Lake Tanganyika), but not sites further east (e.g., Lake Rutundu).

4.4. D-depleted precipitation at Lake Rutundu during the LGM

The 25-kyr record of δD_{precip} from Lake Rutundu shows D-depletion during the LGM (−25.1‰, on average) relative to the late Holocene (−8.8‰ on average during 4-0 ka; Fig. 2E). If the amount effect exerted dominant control on δD_{precip} during the LGM at this site, this would suggest that LGM climate conditions in easternmost Africa were wetter than today. However, as other hydroclimate proxies from previous studies on Mt. Kenya (i.e., fossil pollen, leaf-wax carbon isotopes, grass-cuticle analysis, and sediment composition) suggest local drying during the LGM, the question arises whether other climate processes operating at orbital time scales may have influenced the δD_{precip} signal. For example, Ficken et al. (2002) found increased Poaceae pollen during the LGM (~55 % on average) relative to the late Holocene (~30 % on average), suggesting that the vegetation surrounding Lake Rutundu during the LGM was grass-dominated, likely due to drier conditions (Fig. 4A; Ficken et al., 2002). Similarly, a transition from modestly lower $\delta^{13}C_{wax}$ values during the LGM to more strongly ^{13}C-depleted values in the Holocene may indicate a transition to more C3-dominated local vegetation as a result of wetter conditions during the Holocene (Fig. 4B; Wooller et al., 2003). C4 grass expansion during the LGM may be attributed to lower CO_2 levels (Street-Perrott et al., 2004) or increased moisture stress (Ficken et al., 2002; Street-Perrott et al., 2004; Wooller et al., 2003), as suggested by evidence for increased fire prevalence during the LGM (Wooller et al., 2003). Finally, the basal section of the Lake Rutundu sediment sequence, deposited during the LGM, primarily consists of silty diatomaceous mud, indicating lower lake levels and hence less moisture (Ficken et al., 2002). This is followed by a shift to organic diatomaceous mud with fine sand layers at ~19.2 ka, indicating higher lake levels and an overall wetter environment developing shortly after the onset of deglaciation (Ficken et al., 2002).

Similar trends in vegetation and sediment stratigraphy have also been observed at other lakes on Mt. Kenya, such as nearby Sacred Lake (2,350 m asl). Pollen and grass-cuticle records from Sacred Lake show abundant grass pollen and cuticles deposited during the LGM, transitioning to a greater abundance of montane forest pollen in the Holocene due to wetter conditions (Street-Perrott et al., 2004). The carbon isotopic composition of *n*-alkanes at Sacred Lake shows more ^{13}C-enriched values during the LGM

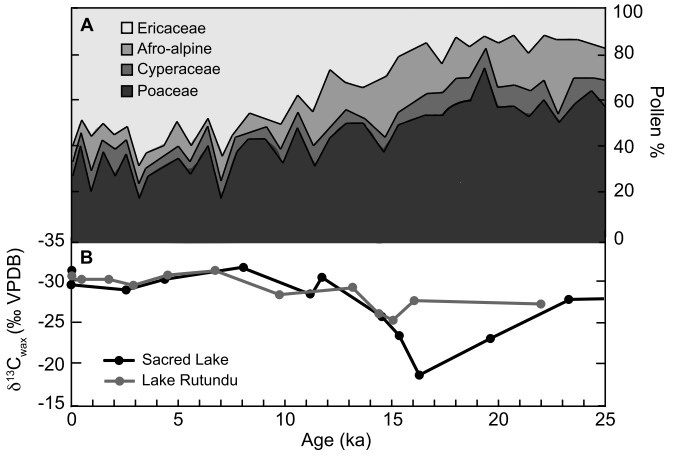

Fig. 4. A) Long-term changes in terrestrial vegetation surrounding Lake Rutundu, reflected in the percent composition of major pollen groups (Ficken et al., 2002). B) $\delta^{13}C_{wax}$ records from Sacred Lake (Huang et al., 1999) and Lake Rutundu (Wooller et al., 2003) on Mt. Kenya, based on weighted-average carbon-isotope values of long-chain leaf-wax *n*-alkanes ($>C_{26}$).

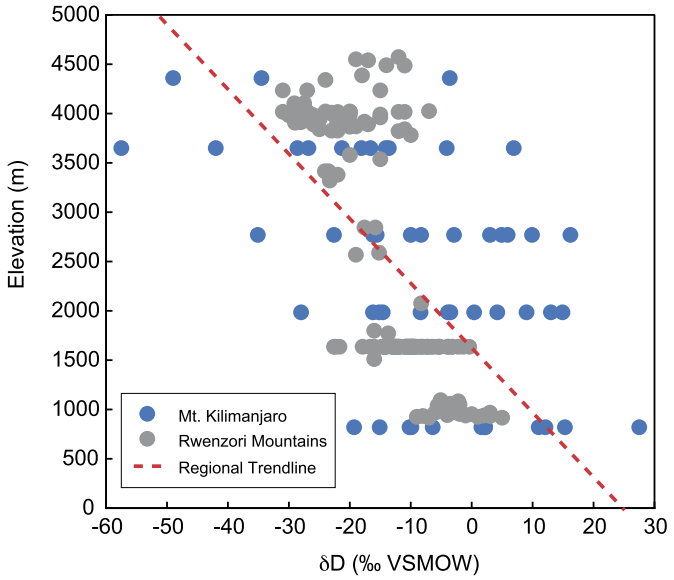

Fig. 5. Modern hydrogen-isotope data from precipitation samples collected along elevational gradients on Mt. Kilimanjaro, Tanzania (blue; Bodé et al., 2019), and surface-water samples in the Rwenzori Mountains, western Uganda (gray; collected by James Russell and collaborators, 1997-2009, unpublished). All data represent single-event samplings across multiple years and seasons, explaining the observed scatter. The linear trend line for all datasets combined (dashed red line; $r^2 = 0.3745$) represents the approximate modern isotopic lapse rate in tropical East Africa and highlights the modern D-depletion at higher elevations.

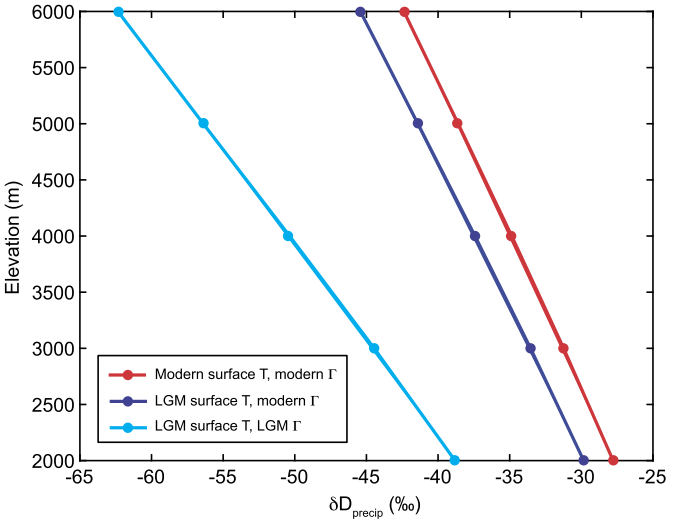

Fig. 6. Results of the single-column Rayleigh distillation model for the three climate scenarios: 'modern surface T, modern Γ' (red), 'LGM surface T, modern Γ' (dark blue), and 'LGM surface T, LGM Γ' (light blue).

than during the Holocene, also indicating a relative expansion of C3 plants (trees and shrubs) after the onset of wetter Holocene conditions (Huang et al., 1999; Fig. 4B). Sedimentological changes recorded by bulk organic matter and magnetic susceptibility data from Sacred Lake also indicate lower lake levels and a drier climate during the LGM (Olago et al., 2000).

Given these multiple lines of evidence for LGM drying on Mt. Kenya, we evaluated causes other than changes in precipitation amount to explain the LGM D-depletion recorded at Lake Rutundu. In modern-day tropical climate regimes, δD_{precip} becomes lower at higher elevations due to Rayleigh distillation and the fractionation associated with upslope vapor transport and condensation (Rowley and Garzione, 2007), and due to temperature-dependent fractionation between vapor and condensate as air masses ascend to higher elevations with lower temperatures (Rowley and Garzione, 2007). This D-depletion at high elevations is clearly exhibited in a compilation of modern-day isotopic composition data from surface-water and precipitation samples collected along altitudinal transects on Mt. Kilimanjaro in Tanzania (Bodé et al., 2019) and in the Rwenzori Mountains in Uganda (James Russell and collaborators, 1997-2009, unpublished). Based on these datasets, the modern-day isotopic lapse rate in eastern equatorial Africa can be inferred to be about −5.7‰/km (Fig. 5).

Our Rayleigh distillation model captures this elevation-dependent D-depletion in precipitation (Fig. 6). In the 'modern surface T, modern Γ' scenario, the model simulates an isotopic lapse rate of −3.7‰/km, slightly shallower than observations. The difference between the modeled and observed modern isotopic lapse rate may be due to a number of effects not included in our model, such as orographic impacts on upslope vapor transport. However, orographic influences likely did not change between the LGM and present. Snowfall at higher elevations is also not included in our model, and would also result in more D-depleted precipitation (Lee et al., 2012). This process could further contribute to the D-depletion we observe at Lake Rutundu during the colder LGM. However, considering that mean annual air temperature at Lake Rutundu is estimated to have been ∼6 °C during the LGM (Loomis et al., 2017), and given limited seasonal temperature variability in the tropics, the majority of precipitation here during the LGM was likely rainfall. Although our model may not produce quantitatively precise isotopic lapse rate values, overall, we infer that it can provide reasonable estimates of the expected isotopic shift due to the change in temperature lapse rate between the LGM and modern alone.

The 'LGM surface T, modern Γ' scenario, with reduced surface temperature and a modern temperature lapse rate, produces a modest surface depletion relative to the 'modern surface T, modern Γ' of approximately −2‰, and an isotopic lapse rate of −3.9‰/km, similar to that of the 'modern surface T, modern Γ' scenario (Fig. 6). In contrast, the 'LGM surface T, LGM Γ' scenario, with both the reduced surface temperature and steeper temperature lapse rate, results in a much larger surface depletion of about −11‰ relative to 'modern surface T, modern Γ' and a steeper isotopic lapse rate of −5.7‰/km (Fig. 6). Specifically, at 3,000 m asl, the approximate elevation of Lake Rutundu, the 'LGM surface T, modern Γ' scenario produces a D-depletion of only −2‰ relative

to 'modern surface T, modern Γ' whereas the 'LGM surface T, LGM Γ' scenario produces a D-depletion of about −13‰ (Fig. 6), a difference an order of magnitude larger.

The relatively strong D-depletion during the LGM observed in the δD_{precip} record from Lake Rutundu is most consistent with our model output for the 'LGM surface T, LGM Γ' scenario, and suggests that the large D-depletion of precipitation at 3,000 m asl primarily results from the steeper temperature lapse rate, rather than LGM cooling alone. This occurs because under a steeper temperature lapse rate, vapor in an ascending air mass condenses more quickly at lower temperatures, enhancing fractionation and hence resulting in isotopically more depleted rainfall. Thus, stronger isotopic depletion of rainfall at high elevations in tropical East Africa during the LGM is to be expected. This amplified Rayleigh distillation and elevation-dependent temperature change may partly explain the LGM D-depletion we observe in our Lake Rutundu δD_{precip} record. Studies of modern precipitation amount and isotopic composition at various elevations on Mt. Kilimanjaro show that the amount effect strongly influences δD_{precip} (Bodé et al., 2019). This is consistent with our interpretations of the Rutundu δD_{precip} record during the deglacial period and Holocene when temperature changes with elevation were relatively small and the temperature lapse rate was likely consistent. The importance of the amount effect today does not preclude a strong isotopic effect of temperature lapse rate during the colder, drier LGM, when the lapse rate was steeper.

In addition to the amount effect, Rayleigh distillation, and the altitudinal temperature gradient, other phenomena may have influenced δD_{precip} during the LGM, including changes in air-mass trajectory, the intensity of convection, and processes associated with water vapor transport, condensation and precipitation (Costa et al., 2014; Konecky et al., 2011). However, as the existence of a steeper temperature lapse rate in tropical Africa during the LGM is supported by both glaciological and organic geochemical evidence (Kelly et al., 2014; Loomis et al., 2017), we propose that amplified Rayleigh distillation due to this steeper temperature lapse rate may have been a dominant influence on LGM δD_{precip} at our high-elevation site. Although there are uncertainties associated with our lapse rate estimates, our simplified, single-column model is not designed to account for all the processes potentially controlling the isotopic composition of local precipitation and therefore cannot produce a precise quantitative estimate of the change in reconstructed δD_{precip} values that occurred on Mt. Kenya during the LGM. However, the model is useful for estimating the sign and approximate magnitude of local change in isotopic composition that could be expected from the change in temperature lapse rate alone, and suggests that these changes could result in considerable D-depletion in precipitation, as seen in our Lake Rutundu δD_{precip} record during the LGM.

The effect of elevation-dependent LGM cooling on precipitation isotope ratios likely influenced δD_{precip} at other sites in the tropics, but to varying degrees depending on site elevation and changes to the temperature lapse rate dependent on the magnitude of regional cooling. However, we do not expect a strong elevation-dependent temperature effect on δD_{precip} during H1, YD, or the Holocene at our site, because temperature changes at all elevations during these intervals were relatively modest compared to the LGM-to-Holocene transition (e.g., Loomis et al., 2017). Although mean annual air temperature at Lake Rutundu reached a minimum during H1 (Loomis et al., 2017), evidence for cooling at this time is lacking in other East African temperature records (e.g., Tierney et al., 2008), and therefore may reflect a local process on this glaciated mountain that would not have impacted the regional atmospheric temperature lapse rate. In combination with the D-depletion observed at Lake Rutundu, our model results provide qualitative support for organic-biomarker based paleotemperature reconstructions in this region that suggest elevation-dependent cooling during the LGM (e.g., Loomis et al., 2017; Tierney et al., 2008). Overall, we conclude that both the Lake Rutundu δD_{precip} record and the available paleoecological data reflect a drier climate and steepened temperature lapse rate on Mt. Kenya during the LGM.

4.5. Spatial pattern of LGM δD_{precip} anomalies across Africa

Spatiotemporal trends in East African δD_{precip} records can provide insight into the larger-scale mechanisms controlling hydroclimate change over Africa. The long-term pattern in the 25-kyr Lake Rutundu δD_{precip} record is generally coherent with patterns observed in other δD_{precip} records from northern and equatorial East Africa, including the Gulf of Aden (Tierney and deMenocal, 2013) and Lake Tanganyika (Tierney et al., 2008), in that it broadly follows temporal variation in NH Summer solstice (June 21) insolation (Fig. 7). Conversely, δD_{precip} records from Lake Malawi (Konecky et al., 2011) and the Zambezi River Delta (Schefuß et al., 2011) in southeastern tropical Africa display a different, and at times opposite, long-term trend, and more closely resemble variations in SH Summer solstice (December 21) insolation (Fig. 7). This similarity between patterns of East African δD_{precip} records and either NH or SH insolation confirms the findings from previous syntheses of hydroclimate proxy data (Gasse, 2000; Verschuren et al., 2009) and climate-model simulations in this region (Otto-Bliesner et al., 2014) that suggest a strong influence of meridional processes on East African hydroclimate since the LGM, foremost of these being the influence of precessional insolation forcing on the latitudinal extent and mean annual position of the ITCZ (Kutzbach and Otto-Bliesner, 1982). The fact that this north-south pattern is apparent among δD_{precip} records from East Africa may indicate that the amount effect is indeed the dominant control on long-term variations in δD_{precip}. However, whereas most δD_{precip} records from northern and tropical East Africa exhibit D-enriched precipitation during the LGM relative to today, suggesting drier LGM conditions, our Lake Runtundu δD_{precip} record shows LGM D-depletion (Fig. 7). Since Lake Rutundu is the only high-elevation δD_{precip} record in East Africa, this regionally anomalous LGM D-depletion suggests that the altitude effect, with a steeper temperature lapse rate during the LGM, likely exerts a strong secondary control on long-term δD_{precip} variability.

Although the greater amplitude of long-term temperature variability at high elevation, and the associated temporal change in temperature lapse rate, impart uncertainty on the degree to which the Lake Rutundu δD_{precip} record reflects variation in precipitation amount, examining the amplitude of δD_{precip} variability allows us to assess any additional influence of zonal climate dynamics on hydroclimate across East Africa. The total variation in δD_{precip} over the past 25 kyr at Lake Rutundu, Lake Tanganyika and the Gulf of Aden all range between ∼40 and 50‰, and there is no clear east-west pattern in the general structure and amplitude of δD_{precip} change at these three sites (Fig. 7), suggesting that changes in zonal climate processes did not exert a dominant influence on East African hydroclimate over this period. Overall, our results suggest that although zonal processes may have had some influence on long-term δD_{precip} trends in this region, the dominant signal in the δD_{precip} records is due to meridional processes. With the exception of a few sites, the hydroclimate signals seen in the δD_{precip} records from easternmost equatorial Africa suggest that meridional processes resulted in an overall drier region during the LGM.

5. Conclusions

A new 25-kyr δD_{precip} reconstruction from Lake Rutundu on Mt. Kenya allowed investigation of potential controls on δD_{precip}

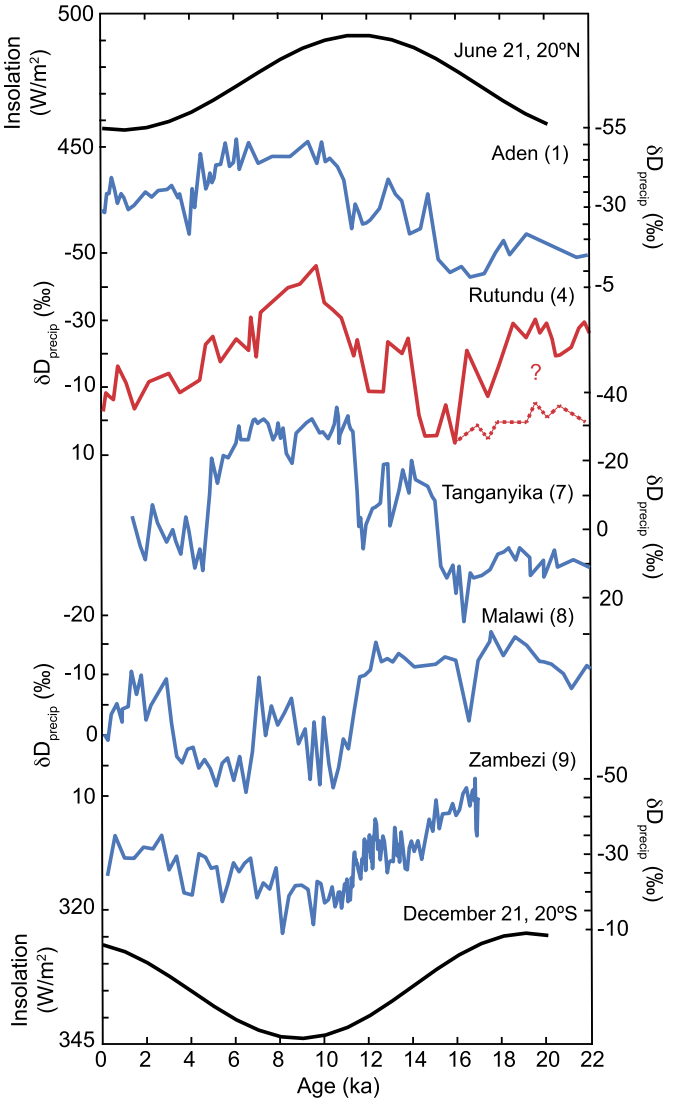

Fig. 7. Selected δD_{precip} records, with values relative to VSMOW, from along a north-to-south transect across East Africa and in relation to NH Summer solstice insolation (June 21 at 20° N) and SH Summer solstice insolation (December 21 at 20° S). The sites are numbered according to their locations in Fig. 1B: Gulf of Aden, Lake Rutundu (the only high-elevation site of the selected locations), Lake Tanganyika, Lake Malawi, and Zambezi River Delta. The dashed line on the Lake Rutundu δD_{precip} record shows one possible temporal trajectory of δD_{precip} at sea level, i.e., after extracting the effect of amplified isotopic depletion on precipitation at high elevations during the LGM. This is not intended to represent a quantitative correction, but a qualitative adjustment to account for increased D-depletion during the LGM caused by elevation-dependent temperature change.

at high-elevation sites in tropical East Africa, and of the large-scale processes controlling hydroclimate variation in this region since the LGM. The Rutundu δD_{precip} record and Rayleigh distillation model presented here suggest that a steeper temperature lapse rate during the LGM amplified the influence of elevation-dependent temperature change on δD_{precip}, causing D-depletion during that time. Explaining this LGM D-depletion by an amplified altitude effect, rather than increased rainfall, resolves the apparent discrepancy between the Lake Rutundu δD_{precip} record and the majority of other proxy data from Mt. Kenya and elsewhere in tropical East Africa indicating regional drying during the LGM. However, uncertainty in the relative influence of the amount effect versus elevation-dependent temperature change on δD_{precip} during the LGM makes it difficult to directly compare our results with other low-elevation records.

More broadly, the relative influence of the altitude effect, depending on changes in temperature lapse rate, affects inferences of past tropical hydroclimate change derived from precipitation isotopes, and should be considered in δD_{precip} reconstructions from sites at all elevations. Production of additional δD_{precip} records from sites in eastern equatorial Africa, particularly at high elevation, may further resolve the controls on δD_{precip} and hydroclimate in this region, and continue to improve paleoclimate data-model comparisons for better prediction of hydroclimate trends associated with future warming in East Africa.

The Lake Rutundu δD_{precip} record displays distinct millennial-scale climate events including drying during the H1 and the YD, as well as gradual termination of the AHP. Comparison of our record with other East African δD_{precip} records reveals the influence of meridional climate-dynamical processes on East African hydroclimate since the LGM, and supports the conclusions of previous regional syntheses that meridional processes, such as changes in the latitudinal migration of the ITCZ due to precessional insolation forcing, exerted dominant control.

CRediT authorship contribution statement

Sloane Garelick: Conceptualization, Formal analysis, Investigation, Writing – original draft. **James M. Russell:** Conceptualization, Funding acquisition, Writing – review & editing. **Sylvia Dee:** Methodology, Writing – review & editing. **Dirk Verschuren:** Resources, Writing – review & editing. **Daniel O. Olago:** Resources, Writing – review & editing.

Declaration of competing interest

The authors declare that they have no known competing financial interests or personal relationships that could have appeared to influence the work reported in this paper.

Acknowledgements

The fieldwork in 1996, which recovered the Rut96 sediment core, was funded by the UK Natural Environment Research Council (grants GT4/96/299/T and GR3/9523). We thank Ngaara Mountaineering Services, the Kenya Wildlife Service, A. Perrott and S.M. Rucina (National Museums of Kenya) for logistic support. Fieldwork in 2009, which recovered the Rut09 core, was sponsored by the Fund of Scientific Research of Flanders (FWO-Vlaanderen) and conducted under permits from the National Council for Science and Technology of Kenya (NCST/RCD/14/012/14), Kenya Wildlife Service (KWS/CL&P/029) and National Environmental Monitoring Authority (NEMA AGR/7/2010) to DV. The core samples were exported for analysis under Material Transfer Agreement (A11/TT/1040) between the Kenya Wildlife Service, the University of Nairobi, and Ghent University. We further thank E. Santos and L. Messier for laboratory assistance. This research is partly supported by National Science Foundation grants NSF-P2C2 1701335 and NSF-P2C2 EAR-1903348 to JMR, and a graduate student fellowship from the Institute at Brown for Environment and Society (IBES, Brown University) to SG.

Appendix A. Supplementary material

Supplementary material related to this article can be found online at https://doi.org/10.1016/j.epsl.2021.116984.

References

Ampuero, A., Stríkis, N.M., Apaéstegui, J., Vuille, M., Novello, V.F., Espinoza, J.C., Cruz, F.W., Vonhof, H., Mayta, V.C., Martins, V.T.S., Cordeiro, R.C., Azevedo, V., Sifeddine, A., 2020. The forest effects on the isotopic composition of rainfall in the northwestern Amazon basin. J. Geophys. Res., Atmos. 125.

Barker, P., Gasse, F., 2003. New evidence for a reduced water balance in East Africa during the Last Glacial Maximum: implication for model-data comparison. Quat. Sci. Rev. 22, 823–837.
Berke, M.A., Johnson, T.C., Werne, J.P., Grice, K., Schouten, S., Damsté, J.S.S., 2012. Molecular records of climate variability and vegetation response since the Late Pleistocene in the Lake Victoria basin, East Africa. Quat. Sci. Rev. 55, 59–74.
Berke, M.A., Johnson, T.C., Werne, J.P., Livingstone, D.A., Grice, K., Schouten, S., Damste, J.S.S., 2014. Characterization of the last deglacial transition in tropical East Africa: insights from Lake Albert. Palaeogeogr. Palaeoclimatol. Palaeoecol. 409, 1–8.
Bodé, S., De Wispelaere, L., Hemp, A., Verschuren, D., Boeckx, P., 2019. Water-isotope ecohydrology of Mount Kilimanjaro. Ecohydrology 13.
Bray, E., Evans, E., 1961. Distribution of n-paraffins as a clue to recognition of source beds. Geochim. Cosmochim. Acta 22, 2–15.
Chen, J., Dai, A., Zhang, Y., Rasmussen, K.L., 2020. Changes in convective available potential energy and convective inhibition under global warming. J. Climate 33, 2025–2050.
Costa, K., Russell, J., Konecky, B., Lamb, H., 2014. Isotopic reconstruction of the African Humid Period and Congo Air Boundary migration at Lake Tana, Ethiopia. Quat. Sci. Rev. 83, 58–67.
Cranwell, P.A., 1973. Chain-length distribution of n-alkanes from lake sediments in relation to post-glacial environmental change. Freshw. Biol. 3, 259–265.
Dansgaard, W., 1964. Stable isotopes in precipitation. Tellus 16, 436–468.
Dee, S.G., Nusbaumer, J., Bailey, A., Russell, J.M., Lee, J.E., Konecky, B., Buenning, N.H., Noone, D.C., 2018. Tracking the strength of the Walker Circulation with stable isotopes in water vapor. J. Geophys. Res., Atmos. 123, 7254–7270.
DiNezio, P.N., Tierney, J.E., Otto-Bliesner, B.L., Timmermann, A., Bhattacharya, T., Rosenbloom, N., Brady, E., 2018. Glacial changes in tropical climate amplified by the Indian Ocean. Sci. Adv. 4, eaat9658.
Ficken, K.J., Wooller, M.J., Swain, D., Street-Perrott, F.A., Eglinton, G., 2002. Reconstruction of a subalpine grass-dominated ecosystem, Lake Rutundu, Mount Kenya: a novel multi-proxy approach. Palaeogeogr. Palaeoclimatol. Palaeoecol. 177, 137–149.
Frankenberg, C., Yoshimura, K., Warneke, T., Aben, I., Butz, A., Deutscher, N., Griffith, D., Hase, F., Notholt, J., Schneider, M., 2009. Dynamic processes governing lower-tropospheric HDO/H2O ratios as observed from space and ground. Science 325, 1374–1377.
Garcin, Y., Vincens, A., Williamson, D., Guiot, J., Buchet, G., 2006. Wet phases in tropical southern Africa during the last glacial period. Geophys. Res. Lett. 33.
Gasse, F., 2000. Hydrological changes in the African tropics since the Last Glacial Maximum. Quat. Sci. Rev. 19, 189–211.
Hodell, D.A., Nicholl, J.A., Bontognali, T.R., Danino, S., Dorador, J., Dowdeswell, J.A., Einsle, J., Kuhlmann, H., Martrat, B., Mleneck-Vautravers, M.J., 2017. Anatomy of Heinrich Layer 1 and its role in the last deglaciation. Paleoceanography 32, 284–303.
Huang, Y., Street-Perrott, F.A., Perrott, R.A., Metzger, P., Eglinton, G., 1999. Glacial-interglacial environmental changes inferred from molecular and compound-specific d13C analyses of sediments from Sacred Lake, Mt. Kenya. Geochim. Cosmochim. Acta 63, 1383–1404.
Kelly, M.A., Russell, J.M., Baber, M.B., Howley, J.A., Loomis, S.E., Zimmerman, S., Nakileza, B., Lukaye, J., 2014. Expanded glaciers during a dry and cold Last Glacial Maximum in equatorial East Africa. Geology 42, 519–522.
Konecky, B., Russell, J., Huang, Y., Vuille, M., Cohen, L., Street-Perrott, F.A., 2014a. Impact of monsoons, temperature, and CO2 on the rainfall and ecosystems of Mt. Kenya during the Common Era. Palaeogeogr. Palaeoclimatol. Palaeoecol. 396, 17–25.
Konecky, B., Russell, J., Vuille, M., Rehfeld, K., 2014b. The Indian Ocean Zonal Mode over the past millennium in observed and modeled precipitation isotopes. Quat. Sci. Rev. 103, 1–18.
Konecky, B., Russell, J., Bijaksana, S., 2016. Glacial aridity in central Indonesia coeval with intensified monsoon circulation. Earth Planet. Sci. Lett. 437, 15–24.
Konecky, B.L., Russell, J.M., Johnson, T.C., Brown, E.T., Berke, M.A., Werne, J.P., Huang, Y., 2011. Atmospheric circulation patterns during late Pleistocene climate changes at Lake Malawi, Africa. Earth Planet. Sci. Lett. 312, 318–326.
Kutzbach, J., Otto-Bliesner, B., 1982. The sensitivity of the African-Asian monsoonal climate to orbital parameter changes for 9000 years BP in a low-resolution general circulation model. J. Atmos. Sci. 39, 1177–1188.
Lee, J.E., Risi, C., Fung, I., Worden, J., Scheepmaker, R.A., Lintner, B., Frankenberg, C., 2012. Asian monsoon hydrometeorology from TES and SCIAMACHY water vapor isotope measurements and LMDZ simulations: implications for speleothem climate record interpretation. J. Geophys. Res., Atmos. 117.
Lisiecki, L.E., Raymo, M.E., 2005. A Pliocene-Pleistocene stack of 57 globally distributed benthic δ18O records. Paleoceanography 20, PA1003.
Loomis, S.E., Russell, J.M., Verschuren, D., Morrill, C., De Cort, G., Sinninghe Damsté, J.S., Olago, D., Eggermont, H., Street-Perrott, F.A., Kelly, M.A., 2017. The tropical lapse rate steepened during the Last Glacial Maximum. Sci. Adv. 3.
Niang, I., Ruppel, O., Abdrabo, M., Essel, A., Lennard, C., Padgham, J., Urquhart, P., 2014. Africa Climate Change 2014: Impacts, Adaptation, and Vulnerability. Part B: Regional Aspects. Contribution of Working Group II to the Fifth Assessment Report of the Intergovernmental Panel on Climate Change ed VR Barros et al. Cambridge Univ Press, Cambridge, UK.
Olago, D., Street-Perrott, F., Perrott, R., Ivanovich, M., Harkness, D., Odada, E., 2000. Long-term temporal characteristics of palaeomonsoon dynamics in equatorial Africa. Glob. Planet. Change 26, 159–171.
Otto-Bliesner, B.L., Russell, J.M., Clark, P.U., Liu, Z., Overpeck, J.T., Konecky, B., de-Menocal, P., Nicholson, S.E., He, F., Lu, Z., 2014. Coherent changes of south-eastern equatorial and northern African rainfall during the last deglaciation. Science 346, 1223–1227.
Rowley, D.B., Garzione, C.N., 2007. Stable isotope-based paleoaltimetry. Annu. Rev. Earth Planet. Sci. 35, 463–508.
Sachse, D., Billault, I., Bowen, G.J., Chikaraishi, Y., Dawson, T.E., Feakins, S.J., Freeman, K.H., Magill, C.R., McInerney, F.A., Van Der Meer, M.T., 2012. Molecular paleohydrology: interpreting the hydrogen-isotopic composition of lipid biomarkers from photosynthesizing organisms. Annu. Rev. Earth Planet. Sci. 40, 221–249.
Schefuß, E., Kuhlmann, H., Mollenhauer, G., Prange, M., Pätzold, J., 2011. Forcing of wet phases in southeast Africa over the past 17,000 years. Nature 480, 509–512.
Schrag, D.P., Adkins, J.F., McIntyre, K., Alexander, J.L., Hodell, D.A., Charles, C.D., McManus, J.F., 2002. The oxygen isotopic composition of seawater during the Last Glacial Maximum. Quat. Sci. Rev. 21, 331–342.
Shanahan, T.M., McKay, N.P., Hughen, K.A., Overpeck, J.T., Otto-Bliesner, B., Heil, C.W., King, J., Scholz, C.A., Peck, J., 2015. The time-transgressive termination of the African Humid Period. Nat. Geosci. 8, 140–144.
Stager, J.C., Ryves, D.B., Chase, B.M., Pausata, F.S., 2011. Catastrophic drought in the Afro-Asian monsoon region during Heinrich event 1. Science 331, 1299–1302.
Street-Perrott, F.A., Ficken, K.J., Huang, Y., Eglinton, G., 2004. Late Quaternary changes in carbon cycling on Mt. Kenya, East Africa: an overview of the δ13C record in lacustrine organic matter. Quat. Sci. Rev. 23, 861–879.
Svensson, A., Andersen, K.K., Bigler, M., Clausen, H.B., Dahl-Jensen, D., Davies, S., Johnsen, S.J., Muscheler, R., Parrenin, F., Rasmussen, S.O., 2008. A 60 000 Year Greenland Stratigraphic Ice Core Chronology.
Talbot, M.R., Filippi, M.L., Jensen, N.B., Tiercelin, J.J., 2007. An abrupt change in the African monsoon at the end of the Younger Dryas. Geochem. Geophys. Geosyst. 8.
Tierney, J.E., deMenocal, P.B., 2013. Abrupt shifts in Horn of Africa hydroclimate since the Last Glacial Maximum. Science 342, 843–846.
Tierney, J.E., Russell, J.M., Huang, Y., Damsté, J.S.S., Hopmans, E.C., Cohen, A.S., 2008. Northern hemisphere controls on tropical southeast African climate during the past 60,000 years. Science 322, 252–255.
Tierney, J.E., Russell, J.M., Damsté, J.S.S., Huang, Y., Verschuren, D., 2011. Late Quaternary behavior of the East African monsoon and the importance of the Congo Air Boundary. Quat. Sci. Rev. 30, 798–807.
Uno, K.T., Polissar, P.J., Kahle, E., Feibel, C., Harmand, S., Roche, H., Demenocal, P.B., 2016. A Pleistocene palaeovegetation record from plant wax biomarkers from the Nachukui Formation, West Turkana, Kenya. Philos. Trans. R. Soc. B, Biol. Sci. 371, 20150235.
Van Bree, L., Peterse, F., Van der Meer, M., Middelburg, J., Negash, A., De Crop, W., Cocquyt, C., Wieringa, J., Verschuren, D., Damsté, J.S., 2018. Seasonal variability in the abundance and stable carbon-isotopic composition of lipid biomarkers in suspended particulate matter from a stratified equatorial lake (Lake Chala, Kenya/Tanzania): Implications for the sedimentary record. Quat. Sci. Rev. 192, 208–224.
Verschuren, D., Damsté, J.S.S., Moernaut, J., Kristen, I., Blaauw, M., Fagot, M., Haug, G.H., 2009. Half-precessional dynamics of monsoon rainfall near the East African Equator. Nature 462, 637–641.
Vuille, M., Werner, M., Bradley, R.S., Chan, R., Keimig, F., 2005. Stable isotopes in East African precipitation record Indian Ocean zonal mode. Geophys. Res. Lett. 32.
Wang, Y.-J., Cheng, H., Edwards, R.L., An, Z., Wu, J., Shen, C.-C., Dorale, J.A., 2001. A high-resolution absolute-dated late Pleistocene monsoon record from Hulu Cave, China. Science 294, 2345–2348.
WaterisotopesDatabase, 2017. http://waterisotopesDB.org. (Accessed 20 January 2020). Query: Country=Kenya, Type=Rivers and Streams.
Wooller, M.J., Swain, D.L., Ficken, K.J., Agnew, A., Street-Perrott, F., Eglinton, G., 2003. Late Quaternary vegetation changes around Lake Rutundu, Mount Kenya, East Africa: evidence from grass cuticles, pollen and stable carbon isotopes. J. Quat. Sci. 18, 3–15.